error caused by the above-mentioned problem, therefore, in prestin observation, 3 OHCs were analyzed simultaneously and the average value was obtained.

The positions of OHCs, i.e., the stereocilia, cuticular plate and lateral wall of OHCs, were defined using the intensity of F-actin labeling. As shown in Figs. 9C and D, the intensity value of F-actin labeling in the OHC depends on the position of the OHC, that is, the stereocilia and lateral wall account for the V-shaped and ring-like areas of the circular and rectangular analytic regions and the cuticular plate occupies the major area of such analytic regions. Therefore, the intensity of the OHC should be the greatest at the cuticular plate and should be smaller at the stereocilia and lateral wall. Hence, the z axial position indicating the greatest fluorescence intensity was defined as the cuticular plate. Two micrometers above the cuticular plate was referred to as the stereocilia and 3 μm below the cuticular plate was defined as the lateral wall.

The intensities of F-actin labeling were obtained at the stereocilia, cuticular plate and lateral wall from 16 OHCs in each organ of Corti, i.e., 5 OHCs in the first row, 6 OHCs in the second row and 5 OHCs in the third row, in case of F-actin observation. Average intensities of F-actin labeling of the 16 OHCs were calculated and normalized by the total value of the maximum intensity of the pixels located in one circular analytic region (4095 × number of pixels located in one circular analytic region = 1.8×10^6).

The intensity of prestin labeling decreased with distance from the cuticular plate because of the fast fluorescence decay of FITC. In case of prestin observation, therefore, the intensities of prestin labeling were obtained at 2–7 μm below the cuticular plate with intervals of 0.5 μm, leading to 11 micrographs, and were averaged. The intensity of prestin labeling was obtained from 9 OHCs in each organ of Corti, i.e., 3 OHCs in the first row, 3 OHCs in the second row and 3 OHCs in the third row. Average intensities of prestin labeling of 9 OHCs were calculated. They were then normalized by one-third of the total value of the maximum intensity of the pixels located in one rectangular analytic region (4095 × number of pixels located in one rectangular analytic region/3 = 1.3×10^7).

The intensity of the labeled specimens corresponds to their amount because the intensity is proportional to the amount of a fluorescent substance specifically conjugated with the specimens when the preparation and the observation are performed under the same conditions. Therefore, in the present study, the intensity of F-actin labeled with rhodamine and the intensity of prestin labeled with FITC represent the amount of F-actin and the amount of prestin, respectively.

4.4. *Protein expression analysis by Western blotting*

4.4.1. *Sample preparation*

Animals were anesthetized with diethylether and subsequently decapitated. Both left and right temporal bones were immediately removed and the bullae were exposed. The bullae were transferred to a Petri dish containing tissue culture medium (Leibovitz's L-15, Invitrogen), and the cochleae were then exposed with tweezers. The cochlea was kept in an Eppendorf tube containing 30 μl of lysis buffer and homogenized by sonication in ice. The lysis buffer consisted of 1% Nonidet P-40 non-ionic detergent (Sigma-Aldrich), 100 μg/ml of phenylmethylsulfonyl fluoride (Sigma-Aldrich) and a 1:50 dilution of proteases inhibitor cocktail (Sigma-Aldrich). Samples were then kept in ice for 1 h for lysis. Samples were centrifuged at 2900×*g*, 4 °C for 10 min to remove nuclei and unlysed cells, and the supernatant was then removed. This supernatant was used as the cochlear sample. Protein concentration of the cochlear sample was then determined by a DC protein assay kit (Bio-Rad Laboratories, Hercules, CA) based on Lowry's method.

4.4.2. *Western blotting*

For Western blotting, 15 μg of total cochlea protein was diluted in sample buffer with 5% β-mercaptoethanol and denatured by boiling for 5 min. Samples were loaded onto sodium dodecyl sulfate (SDS)-10% polyacrylamide gel and transferred to a nitrocellulose membrane. To reduce the measurement error due to Western blotting, all samples were loaded onto the same gel and transferred to the same membrane. The membrane was immersed in a 1:5000 dilution of rabbit anti-HSP25 antibody and a 1:500 dilution of horseradish peroxidase (HRP) labeled goat anti-rabbit IgG. Because mouse HSP25 and HSP27 have amino acid homology of about 98% and HSP25 has a function similar to HSP27 regarding the regulation of actin polymerization, HSP25 is frequently referred to as HSP27 in mice. It has also been reported that anti-HSP25 can recognize rodent HSP27 (Leonova et al., 2002). Therefore, bands of HSP27 on the membrane can be labeled by anti-mouse HSP25 antibody. Immunolabeled bands of HSP27 were visualized by enhanced chemiluminescence (ECL). The intensity of HSP27 bands was then measured. In images of Western blotting, each pixel has an intensity value ranging from 0 (dark) to 4095 (light). A rectangular analytic region which contains 144 pixels was defined so that a band was located there. The summation of the intensity in each pixel within the analytic region was defined as the intensity of the HSP27 band. The intensity of the HSP27 band was then normalized by the total value of the maximum intensity of the pixels located in the analytic region (4095 × 144 = 589,680).

The intensity of protein bands represents the expression level of the protein because the intensity is proportional to the amount of HRP, which emits light due to ECL, specifically conjugated with the protein bands. Therefore, in the present study, the intensity of HSP27 bands represents the expression level of HSP27.

Acknowledgments

This work was supported by Grant-in-Aid for Scientific Research on Priority Areas 15086202 from the Ministry of Education, Culture, Sports, Science and Technology of Japan; Grant-in-Aid for Scientific Research (B) 18390455 from the Japan Society for the Promotion of Science; a Health and Labour Science Research Grant from the Ministry of Health, Labour and Welfare of Japan; Grant-in-Aid for Exploratory Research 18659495 from the Ministry of Education, Culture, Sports, Science and Technology of Japan; a grant from the Human Frontier Science Program; a grant from the Iketani Science and Technology Foundation and a grant from the Daiwa Securities Health Foundation to H.W.; Grant-in-Aid for

JSPS Fellows 19002194 from the Japan Society for the Promotion of Science and Special Research Grants 11170012 and 11180001 from the Tohoku University 21st Century COE Program of the "Future Medical Engineering Based on Bionanotechnology" to M.M. and Grant-in-Aid for Scientific Research (C) 17591774 from the Ministry of Education, Culture, Sports, Science and Technology of Japan to N.Y.

REFERENCES

An, S.S., Laudadio, R.E., Lai, J., Rogers, R.A., Fredberg, J.J., 2002. Stiffness changes in cultured airway smooth muscle cells. Am. J. Physiol. Cell Physiol. 283, C792–C801.

Ashmore, J.F., 1987. A fast motile response in guinea-pig outer hair cells: the cellular basis of the cochlear amplifier. J. Physiol. 388, 323–347.

Brownell, W.E., Bader, C.R., Bertrand, D., de Ribaupierre, Y., 1985. Evoked mechanical responses of isolated cochlear outer hair cells. Science 227, 194–196.

Canlon, B., Borg, E., Flock, A., 1988. Protection against noise trauma by pre-exposure to a low level acoustic stimulus. Hear. Res. 34, 197–200.

Chen, G.-D., 2006. Prestin gene expression in the rat cochlea following intense noise exposure. Hear. Res. 222, 54–61.

Furness, D.N., Katori, Y., Mahendrasingam, S., Hackney, C.M., 2005. Differential distribution of β- and γ-actin in guinea-pig cochlear sensory and supporting cells. Hear. Res. 207, 22–34.

Gottlieb, T.A., Ivanov, I.E., Adesnik, M., Sabatini, D.D., 1993. Actin microfilaments play a critical role in endocytosis at the apical but not the basolateral surface of polarized epithelial cells. J. Cell Biol. 120, 695–710.

Griesinger, C.B., Richards, C.D., Ashmore, J.F., 2004. Apical endocytosis in outer hair cells of the mammalian cochlea. Eur. J. Neurosci. 20, 41–50.

Huang, Z.-W., Luo, Y., Wu, Z., Tao, Z., Jones, R.O., Zhao, H.-B., 2005. Paradoxical enhancement of active cochlear mechanics in long-term administration of salicylate. J. Neurophysiol. 93, 2053–2061.

Kachar, B., Brownell, W.E., Altschuler, R., Fex, J., 1986. Electrokinetic shape changes of cochlear outer hair cells. Nature 322, 365–368.

Laurent, V.M., Fodil, R., Cañadas, P., Féréol, S., Louis, B., Planus, E., Isabey, D., 2003. Partitioning of cortical and deep cytoskeleton responses from transient magnetic bead twisting. Ann. Biomed. Eng. 31, 1263–1278.

Lavoie, J.N., Hickey, E., Weber, L.A., Landry, J., 1993. Modulation of actin microfilament dynamics and fluid phase pinocytosis by phosphorylation of heat shock protein 27. J. Biol. Chem. 268, 24210–24214.

Leger, J.P., Smith, F.M., Currie, R.W., 2000. Confocal microscopic localization of constitutive and heat shock-induced proteins HSP70 and HSP27 in the rat heart. Circulation 102, 1703–1709.

Lei, H., Grinberg, O., Nwaigwe, C.I., Hou, H.G., Williams, H., Swartz, H.M., Dunn, J.F., 2001. The effects of ketamine–xylazine anesthesia on cerebral blood flow and oxygenation observed using nuclear magnetic resonance perfusion imaging and electron paramagnetic resonance oximetry. Brain Res. 913, 174–179.

Leonova, E.V., Fairfield, D.A., Lomax, M.I., Altschuler, R.A., 2002. Constitutive expression of HSP27 in the rat cochlea. Hear. Res. 163, 61–70.

Liberman, M.C., 1987. Chronic ultrastructural changes in acoustic trauma: serial-section reconstruction of stereocilia and cuticular plate. Hear. Res. 26, 65–88.

Liberman, M.C., Beil, D.G., 1979. Hair cell condition and auditory nerve response in normal and noise-damaged cochleas. Acta Oto-Laryngol. 88, 161–176.

Liberman, M.C., Gao, J., He, D.Z.Z., Wu, X., Jia, S., Zuo, J., 2002. Prestin is required for electromotility of the outer hair cell and for the cochlear amplifier. Nature 419, 300–304.

Murakoshi, M., Yoshida, N., Kitsunai, Y., Iida, K., Kumano, S., Suzuki, T., Kobayashi, T., Wada, H., 2006. Effects of heat stress on Young's modulus of outer hair cells in mice. Brain Res. 1107, 121–130.

Oren, R.E., Rasool, N.A., Rubinstein, E.H., 1987. Effect of ketamine on cerebral cortical blood flow and metabolism in rabbits. Stroke 18, 441–444.

Santos-Sacchi, J., Dilger, J.P., 1988. Whole cell currents and mechanical responses of isolated outer hair cells. Hear. Res. 35, 143–150.

Schneider, M., Belyantseva, I.A., Azevedo, R.B., Kachar, B., 2002. Rapid renewal of auditory hair bundles. Nature 418, 837–838.

Schwartz, M., 2004. Rho signaling at a glance. J. Cell Sci. 117, 5457–5458.

Wang, Y., Liberman, M.C., 2002. Restraint stress and protection from acoustic injury in mice. Hear. Res. 165, 96–102.

Weber, T., Zimmermann, U., Winter, H., Mack, A., Köpschall, I., Rohbock, K., Zenner, H.-P., Knipper, M., 2002. Thyroid hormone is a critical determinant for the regulation of the cochlear motor protein prestin. PNAS 99, 2901–2906.

Welch, W.J., 1992. Mammalian stress response: cell physiology, structure/function of stress proteins, and implications for medicine and disease. Physiol. Rev. 72, 1063–1081.

Yoshida, N., Liberman, M.C., 2000. Sound conditioning reduces noise-induced permanent threshold shift in mice. Hear. Res. 148, 213–219.

Yoshida, N., Kristiansen, A., Liberman, M.C., 1999. Heat stress and protection from permanent acoustic injury in mice. J. Neurosci. 19, 10116–10124.

Zhu, M.-L., Yu, N., Zhao, H.-B., 2006. Upregulation of prestin expression in long-term administration of salicylate. Assoc. Res. Otolaryngol. Abs. 373.

Recent Findings on Our Auditory System: It Is Highly Sensitive Owing to the Motility of Sensory Cells

Hiroshi Wada

Department of Bioengineering and Robotics, Tohoku University, 6-6-01 Aoba-yama, Sendai, Japan

(Received; revised; accepted)

Even though the amplitude of tympanic membrane vibrations is only a few nanometers when we speak in a low voice, we can clearly understand what is being said. This is speculated to be due to cochlear amplification. The origin of this amplification is believed to be the motility of mammalian outer hair cells (OHCs), which are located in the organ of Corti of the cochlea. These are the main focuses of this paper. However, firstly, peripheral anatomy is overviewed. Then, the acoustic properties of the outer and middle ears are interpreted. An explanation of the cochlear function follows. Finally, the origin of the motility of OHCs, i.e., the motor protein "prestin," is discussed.

1. INTRODUCTION

The ears are paired sense organs, which collect, transmit, and detect acoustic impulses. Each of them is comprised of three main parts: the outer ear, middle ear, and inner ear. Traveling sound is focused into the external auditory canal by the pinna, causing vibration of the tympanic membrane and motion of the three ossicles in the middle ear. Their motion is transmitted to the cochlea of the inner ear. The mechanical motion of the basilar membrane in the organ of Corti of the cochlea is then transduced into encoded nerve signals in the cochlea, which are transmitted to the brain.

Even though the amplitude of the displacement of tympanic membrane vibrations is only a few nanometers when we speak in a low voice, we can clearly understand what is being said. This is thought to be aided by cochlear amplification caused by the motility of outer hair cells (OHCs), which are located in the organ of Corti. The origin of this motility is believed to be associated with a membrane protein in the lateral wall of OHCs. The gene that codes for this protein has been identified and termed "prestin". Prestin has been found to be a direct voltage-to-force converter, which can operate at microsecond rates.

In this paper, firstly, actual measurement results of the tympanic membrane vibrations are shown. Secondly, the dynamic behavior of the middle ear and the cochlea is presented. Thirdly, the motility of the isolated OHC is demonstrated, and the function of the OHCs, which behave like actuators of mechanical structures, is discussed. Finally, images of prestin obtained by an atomic force microscope are displayed.

2. REMARKABLE SENSITIVITY OF THE EAR

Sound is energy that is transmitted by

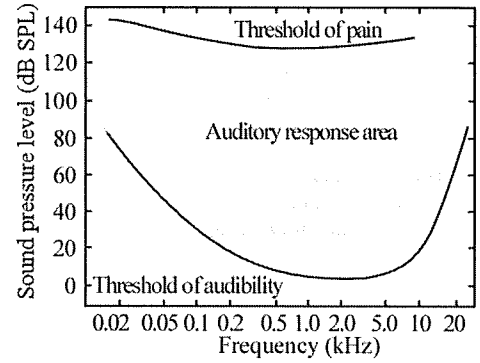

Figure 1. Auditory response area for humans. Sound within the light blue area is audible. This area is bounded on one side by the limits of tolerability of sound and on the other side by the limits of detectability. The difference between the two thresholds is quite wide.

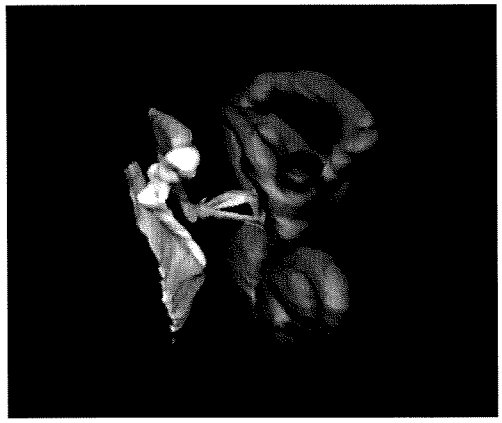

Figure 2. Computer-aided reconstruction of the human middle and inner ear, which was obtained from the temporal bone extracted from a fresh cadaver. The relationship of size and location among the various components can be clearly understood.

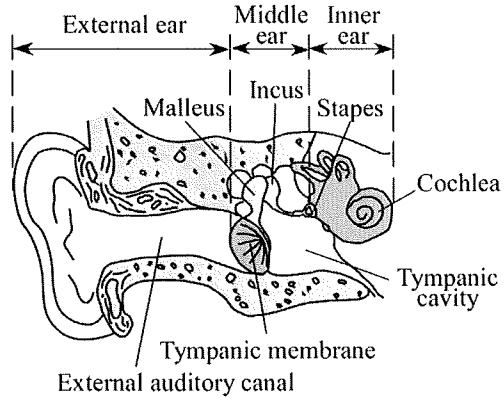

Figure 3. Human peripheral auditory system. Mammals always have three ossicles, namely, the malleus, the incus, and the stapes.

pressure waves in air and is the objective cause of the sensation of hearing. Figure 1 shows the auditory response area for humans [1, 2]. Sound within the light blue area is bounded on one side by the threshold of pain and on the other by the threshold of audibility as a function of frequency. The difference between these thresholds, i.e., the dynamic range, is quite wide, nearly 130 dB SPL at a frequency of 4.0 kHz. High-end recording equipment has a dynamic range of 90 dB. This means that our ears have greater dynamic range than recorded sound.

3. OVERVIEW OF PERIPHERAL ANATOMY: OUTER, MIDDLE, AND INNER EARS

Figure 2 displays a computer-aided reconstruction of the human middle and inner ears, which was obtained from a fixed temporal bone extracted from a fresh cadaver. The relationship of size and location among the various components of the peripheral auditory system can be clearly understood. In humans, as shown in Fig. 3, the external auditory canal with a diameter of 7 mm and a length of 30 mm, which is slightly bent and elliptical, is terminated by a conical-shaped tympanic membrane with a diameter of 10 mm and a thickness of 0.1 mm. Three ossicles, namely, the malleus, incus, and stapes, are located in the tympanic cavity. The malleus is attached to the tympanic membrane, the incus lies between the malleus and the stapes, and the stapes is connected to the cochlea.

Figure 4 depicts the human cochlea with a length of 35 mm, which is spiral-shaped and has three fluid-filled compartments, i.e., the scala vestibuli, the scale media, and the scala tympani. They are separated by Reissner's membrane and the basilar membrane. The scala vestibuli and scala tympani contain perilymph, and the scala media contains endolymph. At the basal end, the scala vestibuli has an oval window and the scala tympani has a round window. The base of the stapes, called the footplate, is sealed by a flexible ligament and transmits the vibration of the middle ear to the fluid in the scala vestibuli.

As shown in Fig. 5, the organ of Corti sits on the basilar membrane and contains two types of hair cells, i.e., the inner hair cells (IHCs) and the OHCs. There are approximately 3,500 IHCs and 12,000 OHCs in humans [3]. Hairlike structures, i.e., stereocilia, extend from the top of these cells. The organ of Corti is covered by the tectorial membrane and given rigidity by the pillar cells. There are three types of supporting cells,

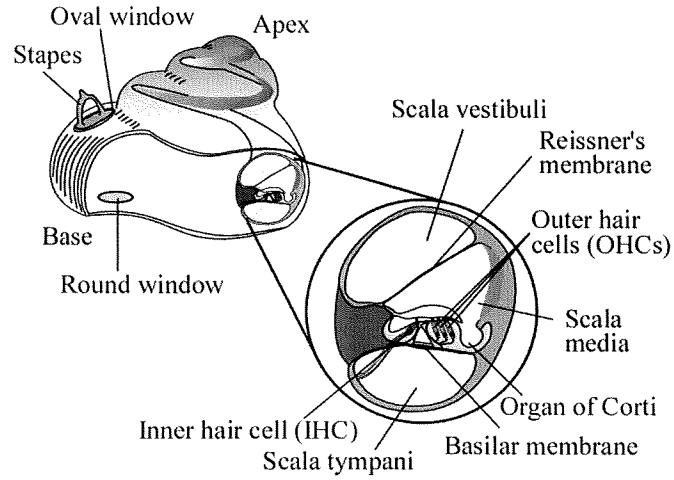

Figure 4. Human cochlea and its cross section. The cochlea has three fluid-filled compartments, which are divided by Reissner's membrane and the basilar membrane.

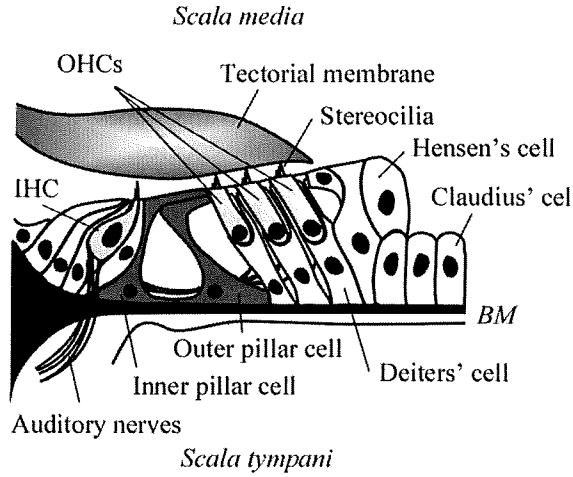

Figure 5. Structure of the organ of Corti. This organ sits on the basilar membrane. Two types of sensory cells, i.e., the inner hair cells (IHCs) and the outer hair cells (OHCs) are located in this organ.

namely, Deiters', Hensen's, and Claudius' cells.

4. ACOUSTICAL PROPERTIES OF THE MIDDLE EAR

Our laboratory measured the vibratory responses of guinea pig tympanic membranes using time-averaged electric speckle pattern interferometry [4]. Figure 6 shows perspective plots of the displacement distribution of the left tympanic membrane vibrations when the displacement at each point reaches its maximum value. The amplitude of tympanic membrane vibrations is between 10 nm and 99 nm (1 nm = 10^{-9} m) when the sound

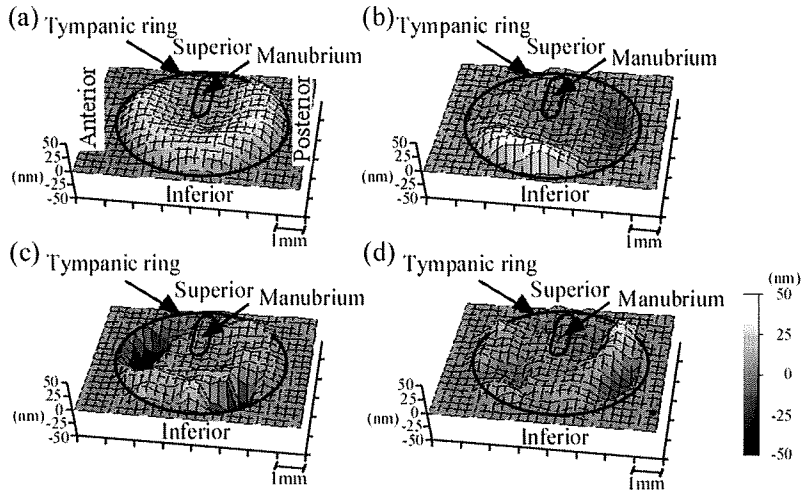

Figure 6. Perspective plots of the displacement distribution of the left tympanic membrane vibrations when the displacement at each point reaches its maximum value. (a) Frequency f = 1.0 kHz and sound pressure level P = 85 dB SPL. (b) f = 2.5 kHz and P = 70 dB SPL. (c) f = 3.0 kHz and P = 75 dB SPL. (d) f = 4.0 kHz and P = 75 dB SPL. At the frequency of 1.0 kHz, the whole tympanic membrane vibrates in phase. The maximum displacement amplitude is about 30 nanometers. At the frequency of 2.5 kHz, the tympanic membrane has two local maxima, one in the posterior portion and the other in the inferior portion. The number of the peaks increases and the vibration mode becomes complicated with an increase in the frequency. From Wada et al. [4]. Copyright © 2002 by The Acoustical Society of America (ASA). Reprinted by permission of American Institute of Physics (on behalf of ASA).

pressure level of the stimulation is between 70 dB SPL and 85 dB SPL.

The three ossicles transmit sound vibrations from the tympanic membrane to the oval window of the cochlea. The main role of the middle ear is to match the low impedance of the air in the external auditory canal to the high impedance of the cochlear fluids. In other words, the middle ear is an impedance transformer. Without this function, much of the sound energy would be reflected. According to our numerical analysis [5, 6], as shown in Fig. 7, the vibration mode of the ossicular chain varies with frequencies. However, as shown in Fig. 8, when the tympanic membrane vibrates, the ossicles basically rotate around the axis between the anterior malleal ligament and the posterior incudal ligament, and the umbo and stapes have a piston-like movement [6, 7]. The area of the tympanic membrane is much larger than that of the stapes footplate. The forces collected by the tympanic membrane, therefore, increase the pressure at the oval window. The arm of the malleus is larger than that of the incus, and this produces leverage, which increases the pressure and decreases the velocity at the stapes. By this mechanism, more than 30% of the sound energy reaches the cochlea.

5. COCHLEAR FUNCTION: TRAVELING WAVES ALONG THE COCHLEAR PARTITION; THE MECHANO-RECEPTOR-TRANSDUCTION ROLE OF HAIR CELLS; RECENT DISCOVERY OF HAIR-CELL MOTILITY, AND THE "COCHLEAR AMPLIFIER"

Vibrations of the stapes generate movement of the cochlear fluids that interacts with the basilar membrane, the stiffness of which decreases from the base to the apex.

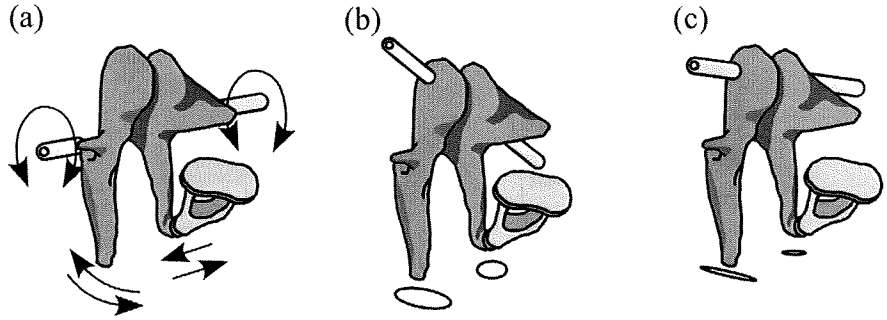

Figure 7. Rotational axis of the ossicular chain. Movements of the tip of the malleus handle and the stapes head are shown by arrows and ellipses. (a) Frequency f = 0.1 kHz. (b) f = 2.0 kHz. (c) f = 4.0 kHz. The rotational axis of the ossicular chain moves to the upper part of the ossicles with an increase in the frequency. From Koike et al. [6]. Copyright © 2002 by The Acoustical Society of America (ASA). Reprinted by permission of American Institute of Physics (on behalf of ASA).

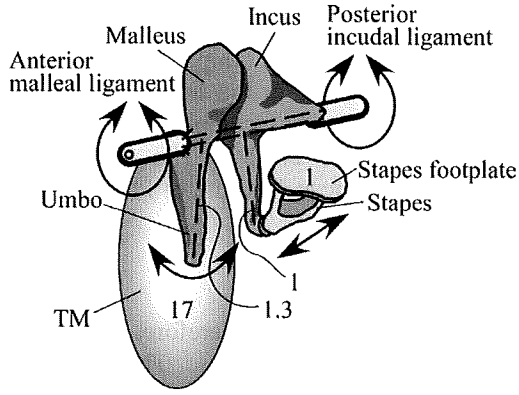

Figure 8. Dynamic behavior of the middle ear. Arrows indicate the directions of the movements. The ratio of the area of the tympanic membrane to that of the stapes is 17:1, and the ratio of the arm of the malleus to that of the incus is 1.3:1.0.

This interaction produces progressive traveling waves on the basilar membrane [8, 9, 10], which are similar to waves beating upon a seashore. Figure 9 depicts these traveling waves [11]. When sound is transmitted to the basilar membrane, the position of the maximum displacement amplitude of its vibration is related to the frequency of the sound. In other words, each position along the basilar membrane has a maximum displacement amplitude at a specific frequency called the characteristic frequency. Figure 10 is afrequency map for humans showing characteristic frequencies at different positions in the ear [12]. As shown in Fig. 11, when sound enters the ear, the organ of Corti, which sits on the basilar membrane, undergoes a rocking motion. Although the details of cochlear operation are unclear, one possible mechanism is that basilar membrane displacement toward the scala vestibuli produces shear motion between the tectorial membrane and the reticular lamina and induces the flow of fluid in the direction of the arrow, which leads to the deflection of the free-standing IHC stereocilia in the same direction as the flow [13, 14]. As shown in Fig. 12, this deflection induces the opening of ion channels and an influx of ions into the IHC, thus releasing the transmitter. As a result, pulses are generated in the auditory nerve fibers, as shown in Fig. 13. Because of this mechanism, we can hear sound.

As depicted in Fig. 14, the mammalian OHC is cylindrical-shaped with a radius of 4-5 μm and a length of 30-90 μm. Similar to the structure of the IHC, the OHC is capped by the cuticular plate with stereocilia at one end and by the synaptic membrane at the other end. When the stereocilia bend in the direction of the arrow, K^+ and Ca^{2+} ions flow into the cell and depolarize the membrane potentials, thereby resembling the function of the IHC.

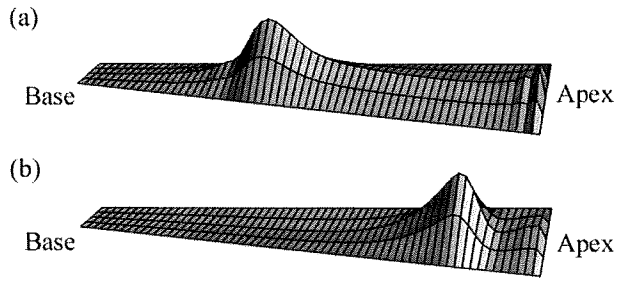

Figure 9. Traveling waves on the basilar membrane obtained by the finite element method model. (a) Input stimulus frequency f = 6.0 kHz. (b) f = 2.0 kHz. Traveling waves on the basilar membrane have a peak near the base when high frequency sound enters the cochlea, while low frequency sound develops the traveling waves on the basilar membrane, which have a peak near the apex.

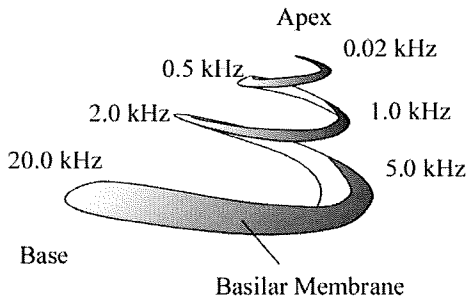

Figure 10. Place-characteristic frequency map for humans. High and low frequency components of sound are analyzed in the basal and apical regions of the cochlea, respectively.

At the same time, the OHC contracts, whereas the IHC releases the transmitter and action potentials are produced in the auditory nerve fibers. When the stereocilia bend in the direction opposite that of the arrow, the membrane potentials are hyperpolarized and the OHC elongates [16]. Figure 15 depicts an experiment where, instead of bending stereocilia, intracellular potentials are charged by the whole-cell voltage clamp technique. Experiments have revealed that the input-output function of the OHC is not expressed by a straight line but a curved one, i.e., the function is non-linear, which is responsible for compressive nonlinear responses of the basilar membrane [17] and the cochlea [18]. Not only the displacement of the OHC but also its stiffness are potential dependent [19]. Moreover, the OHCs are under efferent control [20].

As shown in Fig. 11, when the organ of Corti is deflected toward the scala vestibuli, the OHC stereocilia bend due to the shear motion between the tectorial membrane and the reticular lamina because the tallest OHC stereocilia adhere to the tectorial membrane. Simultaneously, the OHCs contract. Deflection of the organ of Corti toward the scale tympani leads to elongation of the OHCs. This repeated contraction and elongation of the OHCs, i.e., the motility of the OHCs, magnifies the deflection of the organ of Corti. This is said to be a mechanical feedback process [21]. To test the effect of turning off metabolism of the cochlea, we directly measured the basilar membrane vibrations in both living and dead guinea pigs by a laser Doppler velocimeter [22]. Figure 16 clearly shows that amplification of the basilar membrane vibrations occurs when an animal is alive. The magnified deflection of the organ of Corti leads to increases in the movement of the fluids in the space near the stereocilia of the IHCs and in the deflection of the IHC stereocilia. Owing to the mechanism mentioned above, our auditory system is characterized by high sensitivity, sharp tuning, and compressive nonlinearity [23–26]. Recently, not only somatic change but also active hair bundle motion of the OHCs have

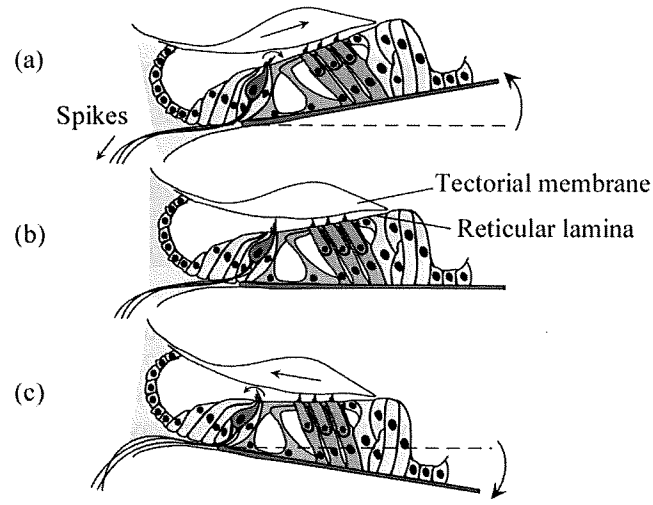

Figure 11. Vibration mode of the organ of Corti. (a) Displacement toward the scala vestibuli. (b) Resting position. (c) Displacement toward the scala tympani. The inner hair cell stereocilia are deflected by the flow of fluid caused by shear motion between the tectorial membrane and the reticular lamina.

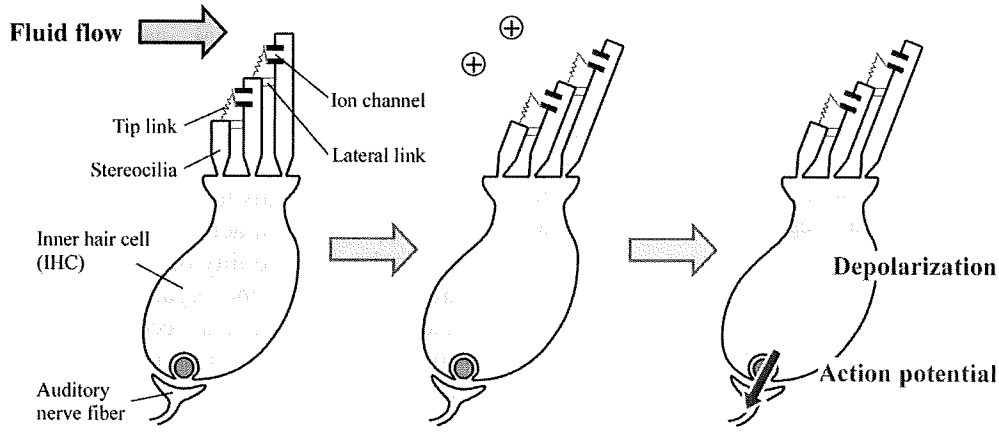

Figure 12. A bundle of stereocilia located on the apical surface of the IHC is deflected by the shear force caused by shear motion of the tectorial membrane against the reticular lamina. When the bundle is deflected in the excitatory direction, i.e., toward the tallest stereocilium, the tip link is under tension and the mechanoelectrical transduction channel located at the end of the tip link is thought to open [15]. Due to this, an influx of ions into the IHC is generated, which in turn depolarizes the membrane potential of the IHC and then produces action potentials in the auditory nerve fibers.

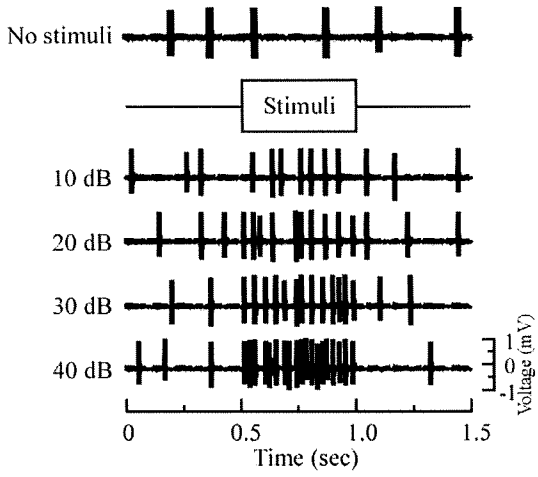

Figure 13. Response in the auditory nerve fiber. The upper waveform is an example of spontaneous activity. When a stimulus tone is delivered to the external auditory canal, the spike rate rises with an increase in the stimulus level.

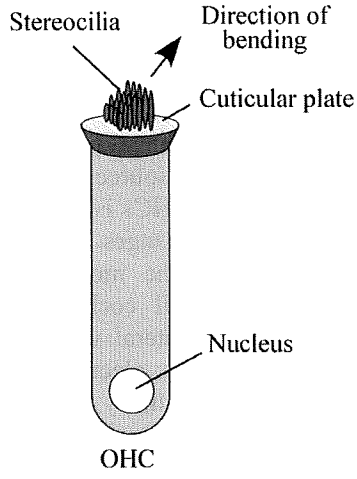

Figure 14. Schematic diagram of the outer hair cell. The polarity is the same as that of Fig. 11. The cell is capped by the cuticular plate with stereocilia, which have a V or W-shaped formation.

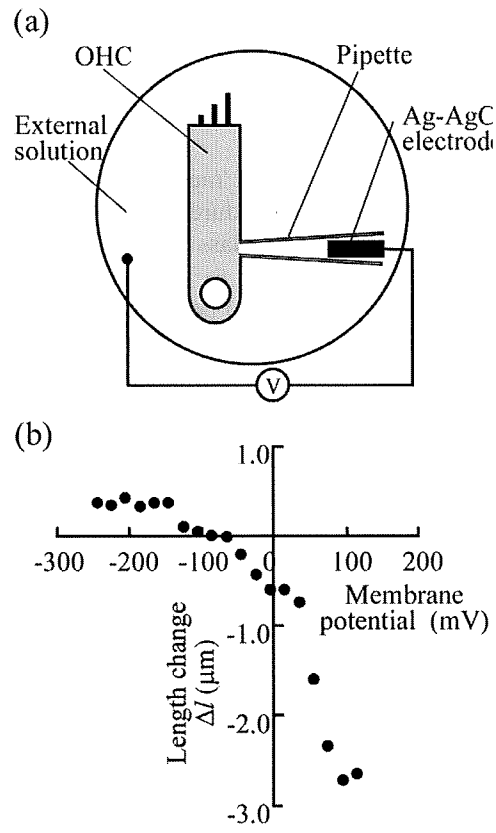

Figure 15. Measurement of outer hair cell motility. (a) Whole-cell voltage clamp technique. To elicit mechanical movement of the outer hair cells, step and sinusoidal voltage stimuli are given to the isolated outer hair cells. (b) Length change of the outer hair cell in response to step voltage stimuli. The positive and negative directions show cell elongation and contraction, respectively.

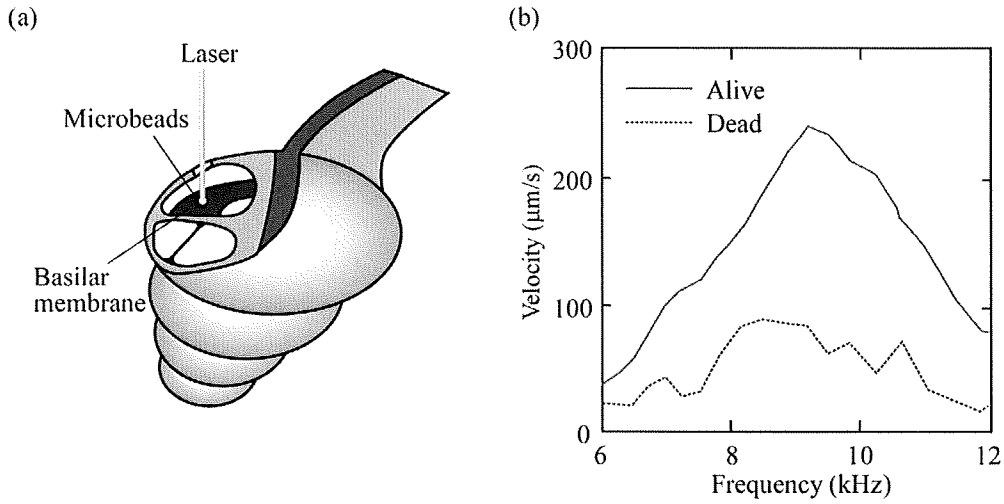

Figure 16. Direct measurement of basilar membrane vibrations in a guinea pig. (a) Measurement procedure. A hole with a diameter of 0.5 mm is opened in the bony wall of the cochlea, and glass microbeads with a diameter of 20 μm are placed on the basilar membrane in order to increase reflections of the laser beam. (b) The basilar membrane velocity responses to periodic tone. P = 75 dB SPL. The basilar membrane vibrations are amplified when an animal is alive.

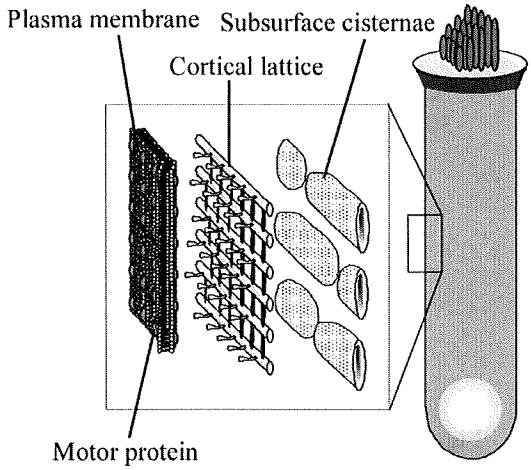

Figure 17. Lateral wall of the OHC. The OHC lateral wall has a unique trilaminate structure: the outermost plasma membrane, the cortical lattice, and the innermost subsurface cisternae. The motor protein is thought to be embedded in the plasma membrane.

been reported [27, 28].

6. THE ORIGIN OF THE MOTILITY OF OHCS, I.E., THE MOTOR PROTEIN "PRESTIN"

As shown in Fig. 17, motor proteins are thought to be embedded in the lateral plasma membrane of the OHCs. The source of the somatic length change of the OHCs is considered to be the conformational changes of these motor proteins. In 2000, the motor protein was identified in the gerbil cochlea and termed "prestin" [29]. The lateral wall of the OHC has been observed by electron microscopy. The existence of many particles, ten nanometers in diameter, in the plasma membrane has been shown using the freeze-fracture technique [30–32]. These densely packed 10-nm particles in the lateral membrane of OHCs are thought to be motor proteins. However, it still remains unknown whether these particles are prestin or not.

The cytoplasmic surfaces of isolated plasma membranes of the prestin-transfected Chinese hamster ovary (CHO) cells and those

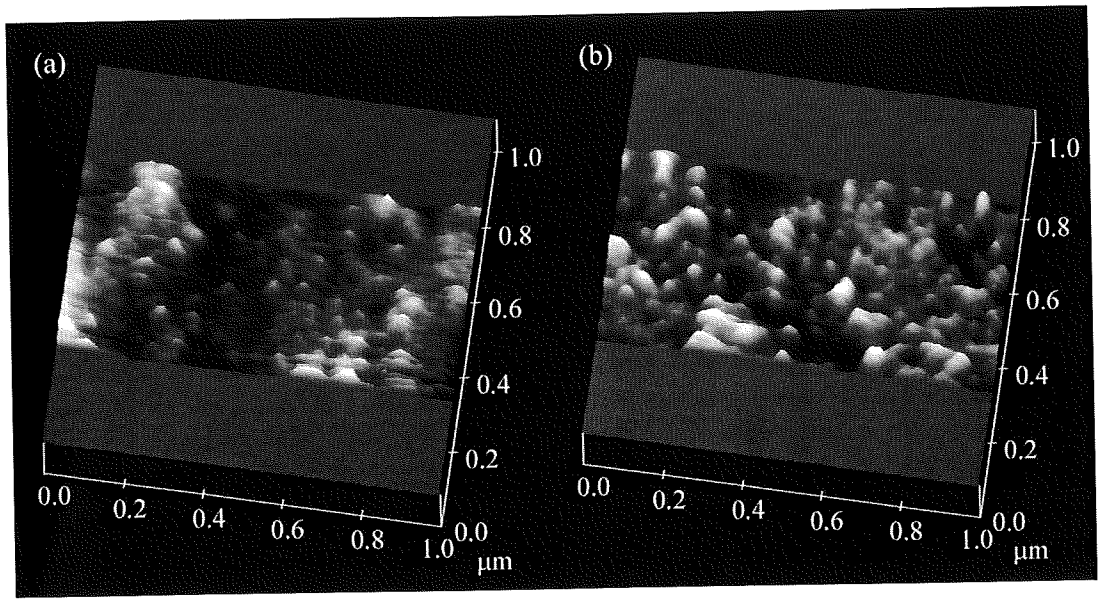

Figure 18. Three-dimensional topographies of the cytoplasmic faces of isolated plasma membranes of the CHO cells observed by AFM in liquid. (a) Untransfected CHO cell. (b) Prestin-transfected CHO cell. More particle-like structures with a diameter of 8–12 nm exist in the plasma membrane of the prestin-transfected CHO cell than in that of the untransfected CHO cell, suggesting that these structures are possibly constituted only by prestin molecules.

of untransfected CHO cells were therefore observed by the tapping mode of AFM to visualize the membrane proteins [33, 34]. Figure 18 represents their AFM images. Analysis of the shape and size of the observed structures was then performed using AFM images of the prestin-transfected CHO cells and those of the untransfected CHO cells. The frequency distribution of the observed particle-like structures, i.e., the density of the particle-like structures plotted against the interval of 2-nm classes in the diameter, is shown in Fig. 19. Since the difference between the prestin-transfected and untransfected CHO cells is due to the existence of prestin, the difference of the densities of the particle-like structures between the prestin-transfected CHO cells and the untransfected CHO cells is considered to be caused by the presence or absence of prestin. Based on Fig. 19, therefore, the density of prestin in the prestin-transfected CHO cells was estimated to be 18 ± 9 proteins/μm^2 (n = 5) after subtracting the value of the density of the particle-like structures in the untransfected CHO cells from those in the prestin-transfected CHO cells in the 8–12 nm class. This value corresponds to approximately 75% of the total density of the particle-like structures in the prestin-transfected CHO cell membrane. These results suggest that the majority of these particle-like structures with a diameter of 8–12 nm in the prestin-transfected CHO plasma membrane are possibly prestin.

7. CONCLUSIONS

An anatomical and functional overview of the human auditory system was herein presented, the main conclusions being as follows: High sensitivity and sharp tuning of our auditory system originate in the motility of the outer hair cells located in the organ of Corti in the cochlea, the source of this motility is the conformational changes of the motor protein prestin in the lateral wall of the cells, and the input-output function of the outer hair cell motility governs the non-linearity of our

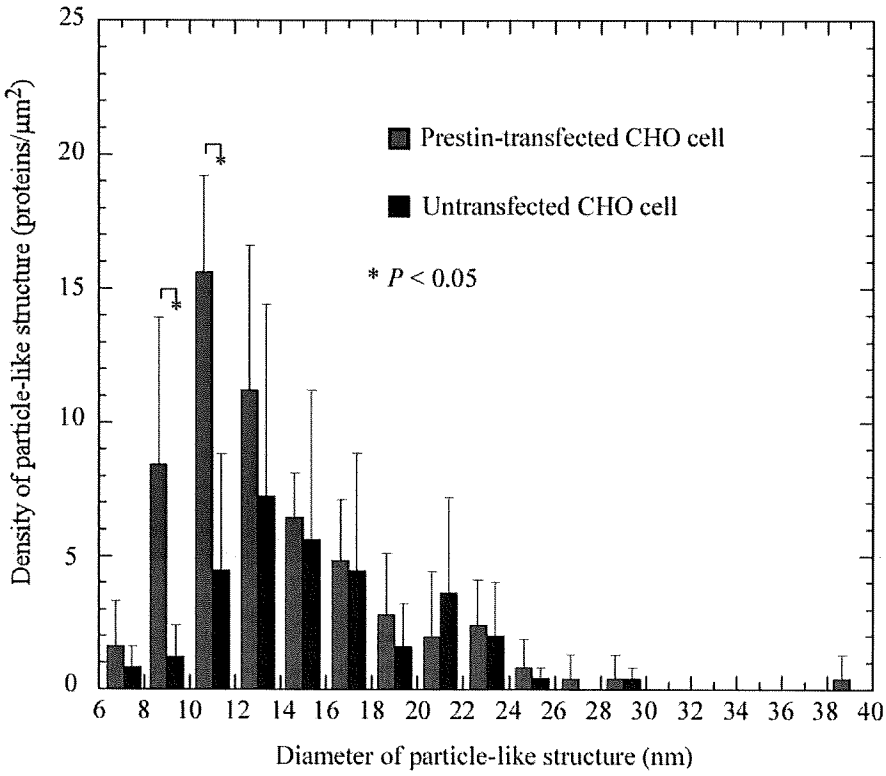

Figure 19. Frequency distribution of the observed particle-like structures in the plasma membrane. The density of the particle-like structures is plotted against the interval in 2-nm classes. Data were obtained from five AFM images of prestin-transfected CHO cells and five such images of untransfected CHO cells. When the sizes of the particle-like structures were 8–10 nm and 10–12 nm, differences of their densities between the prestin-transfected CHO cells and the untransfected CHO cells were statistically significant for $P < 0.05$ using Student's *t*-test, as shown by the asterisks. Error bars represent standard deviations. From Murakoshi et al. [34]. Copyright © 2006 by Springer. Reprinted by permission of Springer.

auditory system.

REFERENCES

[1] W. M. Robinson and R. S. Dadson, A redetermination of the equal loudness relations for pure tones, *Br. J. Appl. Phys.*, **7**(5), 166-181, (1956).

[2] R. L. Wegel, Physical data and physiology of excitation of the auditory nerve, *Ann. Otol. Rhinol. Laryngol.*, **41**, 740-779, (1932).

[3] L. Ulehlova, L. Voldrich and R. Janisch, Correlative study of sensory cell density and cochlea length in humans, *Hear. Res.*, **28**(2-3), 149-151, (1987).

[4] H. Wada, M. Andoh, M. Takeuchi, H. Sugawara, T. Koike, T. Kobayashi, K. Hozawa, T. Gemma and M. Nara, Vibration measurement of the tympanic membrane of guinea pig temporal bones using time-averaged speckle pattern interferometry, *J. Acoust. Soc. Am.*, **111**(5), 2189-2199, (2002).

[5] T. Koike, H. Wada, T. Kobayashi, K. Ohyama and T. Takasaka, Theoretical analysis of sound transmission in human middle ear and its effects on otoacoustic emissions. In: H. Wada et al. (eds.), Recent Developments in Auditory Mechanics, World Scientific Publishing, Singapore, 71-77, (2000).

[6] T. Koike, H. Wada and T. Kobayashi, Modeling of the human middle ear using the finite-element method, *J. Acoust. Soc. Am.*, **111**(3), 1306-1317, (2002).

[7] W. F. Decraemer and S. M. Khanna, New insights into vibration of the middle ear. In: J. J. Rosowski and S. N. Merchant (eds.), The Function and Mechanics of Normal, Diseased and Reconstructed Middle Ears, Kluwer, The Hague, 23-38 , (2000).

[8] G. V. Békésy, *Experiments in Hearing,* McGraw-Hill Book Company, Inc., New York, 452-455, (1960).

[9] O. F. Ranke, Theory of operation of the cochlea: A contribution to the hydrodynamics of the cochlea, *J. Acoust. Soc. Am.*, **22**(6), 772-777, (1950).

[10] W. M. Siebert, Ranke revisited—a simple short-wave cochlear model, *J. Acoust. Soc. Am.*, **56**(2), 594-600, (1974).

[11] Wada Laboratory, Dynamic animation of the basilar membrane, Available at: http://www.wadalab.mech.tohoku.ac.jp/.

[12] G. V. Békésy, *Experiments in Hearing,* McGraw-Hill Book Company, Inc., New York, 441-443, (1960).

[13] H. Wada, A. Takeda and T. Kawase, Timing of neural excitation in relation to basilar membrane motion in the basal region of the guinea pig cochlea during the presentation of low-frequency acoustic stimulation, *Hear. Res.*, **165**(1-2), 165-176, (2002).

[14] M. Andoh, C. Nakajima and H. Wada, Phase of neural excitation relative to basilar membrane motion in the organ of Corti: Theoretical considerations, *J. Acoust. Soc. Am.*, **118**(3), 1554-1565, (2005).

[15] J. O. Pickles, S. D. Comis and M .P. Osborne, Cross-links between stereocilia in the guinea pig organ of Corti, and their possible relation to sensory transduction, *Hear. Res.*, **15**(2), 103–112, (1984).

[16] W. E. Brownell, C. R. Bader, D. Bertrand, Y. de Ribaupierre, Evoked mechanical responses of isolated cochlear outer hair cells, *Science*, **227**, 194-196, (1985).

[17] L. Robles, M. A. Ruggero and N. C. Rich, Basilar membrane mechanics at the base of the chinchilla cochlea. I. Input–output functions, tuning curves, and response phases, *J. Acoust. Soc. Am.*, **80**(5), 1364-1374, (1986).

[18] A. Cohen and M. Furst, Integration of outer hair cell activity in a one-dimensional cochlear model, *J. Acoust. Soc. Am.*, **115**(5), 2185-2192, (2004).

[19] P. Dallos and D.Z.Z. He, Two models of outer hair cell stiffness and motility, *J. Assoc. Res. Otolaryngol.*, **1**(4),283-291, (2000).

[20] E. Murugasu and I. J. Russell, The effect of efferent stimulation on basilar membrane displacement in the basal turn of the guinea pig cochlea, *J. Neurosci.*, **16**, 1306-1317, (1996).

[21] P. Dallos, The active cochlea, *J. Neurosci.*, **12**(12), 4575-4585, (1992).

[22] H. Wada, Y. Honnma, S. Takahashi, T. Takasaka and K. Ohyama, Simultaneous measurement of DPOAEs and basilar membrane vibration by acoustic probe and laser Doppler velocimeter. In: E. R. Lewis et al. (eds.), Diversity in Auditory Mechanics, World Scientific Publishing, Singapore, 284-290, (1997).

[23] J. O. Pickles, *An Introduction to the Physiology of Hearing,* Academic Press, London, 136-157, (1988).

[24] C. D. Geisler, *From Sound to Synapse,* Oxford University Press, New York, 125-138, (1998).

[25] J. L. Goldstein, Auditory nonlinearity, *J. Acoust. Soc. Am.*, **41**, 676-689, (1867).

[26] P. Dallos and and B.N. Evans, High-frequency motility of outer hair cells and the cochlear amplifier, *Science*, **267**(5206), 2006–2009, (1995).

[27] R. Fettiplace, Active hair bundle movements in auditory hair cells, *J. Physiol.*, **576**(1), 29–36, (2006).

[28] P. Dallos, J. Zheng and M.A. Cheatham, Prestin and the cochlear amplifier, *J. Physiol.*, **576**(1), 37–42, (2006).

[29] J. Zheng, W. Shen, D. Z. Z. He, K. B. Long, L. D. Madison and P. Dallos, Prestin is the motor protein of cochlear outer hair cells, *Nature*, **405**(6783), 149–155, (2000).

[30] T. Arima, A. Kuraoka, R. Toriya, Y. Shibata and T. Uemura, Quick-freeze, deep-etch visualization of the 'cytoskeletal spring' of cochlear outer hair cells, *Cell Tissue Res.*, **263**(1), 91–97, (1991).

[31] A. Forge, Structural features of the lateral walls in mammalian cochlear outer hair cells, *Cell Tissue Res.*, **265**(3), 473–483, (1991).

[32] F. Kalinec, M. C. Holley, K. H. Iwasa, D. J. Lim and B. Kachar, A membrane-based force generation mechanism in auditory sensory cells, *Proc. Natl. Acad. Sci. U.S.A.*, **89**(18), 8671–8675, (1992).

[33] K. Iida, K. Tsumoto, K. Ikeda, I. Kumagai, T. Kobayashi and H. Wada, Construction of an expression system for the motor protein prestin in Chinese hamster ovary cells, *Hear. Res.*, **205**(1-2), 262-270, (2005).

[34] M. Murakoshi, T. Gomi, K. Iida, S. Kumano, K. Tsumoto, I. Kumagai, K. Ikeda, T. Kobayashi and H. Wada, Imaging by atomic force microscopy of the plasma membrane of prestin-transfected Chinese hamster ovary cells, *J. Assoc. Res. Otolaryngol.*, **7**(3), 267-278, (2006).

Journal of Neuroscience Research 86:1758–1767 (2008)

Bone Marrow-Derived Cells Expressing Iba1 Are Constitutively Present as Resident Tissue Macrophages in the Mouse Cochlea

Takayuki Okano,[1] Takayuki Nakagawa,[1]* Tomoko Kita,[1,2] Shinpei Kada,[1] Momoko Yoshimoto,[3] Tatsutoshi Nakahata,[3] and Juichi Ito[1]

[1]Department of Otolaryngology, Head and Neck Surgery, Graduate School of Medicine, Kyoto University, Kyoto, Japan
[2]Laboratory for Sensory Development, Center for Developmental Biology, RIKEN, Kobe, Japan
[3]Department of Pediatrics, Graduate School of Medicine, Kyoto University, Kyoto, Japan

Immune-mediated inner ear disorder has been well established as a clinical entity; however, the innate immune system of the inner ear is a poorly understood area of research with high clinical and immunological importance. Although the presence of resident tissue macrophages in the inner ear has been suggested, there has been some controversy. In this study, we analyzed the origin of cochlear resident macrophages and the contribution of hematopoietic bone marrow (BM) to the recruitment of macrophages in the cochlea. To visualize the localization of BM-derived cells, BM chimeric mice were made by transplantation of hematopoietic stem cells, which were genetically labeled with enhanced green fluorescent protein, into lethally irradiated C57BL/6 mice. The distribution and characteristics of BM-derived cells in the mouse cochlea were studied immunohistochemically. We successfully identified the constitutive presence of tissue resident macrophages in the spiral ligament and spiral ganglion that are derived from BM in larger numbers than previously reported. Moreover, cochlear resident macrophages gradually turn over for several months during steady-state replacement by BM-derived cells, and the number of cochlear macrophages immediately increased in response to local surgical stress. The present findings demonstrate the hematopoietic origin of cochlear resident and infiltrating macrophages. Our study provides a novel anatomical and immunological basis for the inner ear and indicates that the cochlear resident macrophages would be a therapeutic target in inner ear disorders.

Key words: hematopoietic stem cell; microglia; innate immunity; inner ear

Macrophages are generally considered to be derived from circulating monocytes and roughly classified into two categories; 1) infiltrating macrophages, which migrate from the circulation into tissues in response to inflammatory signals, and 2) resident tissue macrophages, which are present in tissues during steady-state conditions. Resident tissue macrophages take up residence in virtually every tissue of the body and have a broad role in the innate immune system. Recent studies have demonstrated multiple key functions of resident tissue macrophages not only in phagocytosis of foreign bodies or senescent cells but also in the production and secretion of cytokines and the regulation of specific immune responses (Gordon and Taylor, 2005).

The inner ear was once believed to be an immunoprivileged organ isolated by the blood–labyrinthine barrier similar to the central nervous system (CNS) and the cornea and retina of the eye. Although immune-mediated inner ear disorders have been well established as a clinical entity with progressive and fluctuating bilateral sensorineural hearing loss (SNHL), the innate immune system of the inner ear is a poorly understood area of research with high clinical and immunological importance. Recently, Hirose et al. (2005) reported the existence of mononuclear phagocytes in the spiral ligament of nonnoise-exposed CX3CR1$^{GFP/GFP}$ transgenic mice, and the density of CD45-positive cells in the cochlea was quite different between wild-type and transgenic mice used in the study. Lang et al. (2006) also reported that bone marrow (BM)-derived cells are present in the noninjured inner ear of BM chimeric mice and that 5% of BM-derived cells are macrophages dual-labeled with CD45R and/or F4/80. However, the phenotypes shown by BM-derived cells in the inner ear are as yet only partially understood. Whereas previous studies have reported macrophages infiltrating into the coch-

Contract grant sponsor: Ministry of Education, Culture, Sports, Science and Technology of Japan (to T.N., J.I.); Contract grant sponsor: Takeda Science Foundation (to T.N.).

*Correspondence to: Takayuki Nakagawa, MD, PhD, Department of Otolaryngology, Head and Neck Surgery, Graduate School of Medicine, Kyoto University, Kawaharacho 54, Shogoin, Sakyo-ku, 606-8507 Kyoto, Japan. E-mail: tnakagawa@ent.kuhp.kyoto-u.ac.jp

Received 17 June 2007; Revised 2 November 2007; Accepted 14 November 2007

Published online 5 February 2008 in Wiley InterScience (www.interscience.wiley.com). DOI: 10.1002/jnr.21625

lear fluid space in various experimental models, or suggested the presence of resident tissue macrophages in the inner ear, there has been some controversy on the distribution and phenotype of resident tissue macrophages in the inner ear.

A good understanding of the origins and distribution of the resident tissue macrophages in the inner ear, as well as the timing and context of their recruitment, will be essential to understanding the pathogenesis of inner ear immune disorders in which a loss of tissue homeostasis might result from dysfunction of resident tissue macrophages. The aims of the present study were to establish the distribution and phenotype of resident macrophages in the cochlea and to test the contribution of hematopoietic BM to the recruitment of cochlear macrophages.

BM chimeric mice were made by transplantation of hematopoietic stem cells (HSCs) from enhanced green fluorescent protein (EGFP)-transgenic mice into irradiated adult wild-type mice, and the distribution of BM-derived cells in the cochlea was traced. Immunohistochemistry was employed to determine the phenotype of BM-derived cells. The mobilization of cochlear macrophages was tested by using systemic application of macrophage colony-stimulating factor (M-CSF), the primary regulator of the activation of mononuclear phagocytes. We also examined the response of cochlear macrophages to local surgical invasion, used as a model for an acute, local, exogenous stress on the inner ear.

MATERIALS AND METHODS

Animals

Male C57BL/6 mice were purchased from Japan SLC, Inc (Shizuoka, Japan). EGFP transgenic mice [B6;C3-Tg(ACtb-EGFP)CX-FM139Osb] were used as a source of HSCs (Okabe et al., 1997). The animals were maintained in a specific pathogen-free microisolator environment in the Institute of Laboratory Animals, Kyoto University Graduate School of Medicine. All experimental protocols were approved by the Animal Research Committee, Kyoto University Graduate School of Medicine, and conducted in accordance with the NIH *Guide for the care and use of laboratory animals.*

BM Chimeric Mice

HSCs were collected as lineage marker (Lin)-negative, c-kit (CD117)-positive, stem cell antigen 1 (Sca1)-positive cells from the BM of EGFP transgenic mice via cell sorting on a FACS Vantage (Becton-Dickinson, San Jose, CA) as described previously (Yoshimoto et al., 2003). Briefly, whole BM cells were isolated from the femurs and tibiae of EGFP transgenic mice (8–12 weeks of age). BM mononuclear cells were labeled with a primary antibody cocktail (BD Pharmingen, San Diego, CA) for CD3 (145-2C11), B220/CD45R (RA3-6B2), Mac-1 (M1/70), Gr-1 (RB6-8C5), and TER119 (TR119). Lineage-depleted cells (Lin^- cells) were obtained by using auto-MACS (Militenyi Biotec, Bergish Gladbach, Germany). $Lin^-/c\text{-}kit^+/Sca1^+$ cells were collected by cell sorting on a FACS Vantage as HSCs using R-PE-conjugated anti-mouse Ly-6A/E (Sca-1; clone: E13-161.7; BD Pharmingen) and APC-conjugated anti-mouse CD117 (c-Kit; clone: 2B8; BD Pharmingen). C57BL/6 mice (n = 6, 10–12 weeks of age) were irradiated with 9.5 Gy gamma rays (Gamma Cell 40 Exactor; MDS Nordion Inc., Ottawa, Ontario, Canada) and each received 5×10^3 HSCs through the tail vein. At 1 (four ears from two animals), 2 (four ears from two animals), or 4 weeks (four ears from two animals) and 3 (6 ears from 6 animals), or 6 months (six ears from six animals) after transplantation, the temporal bones were dissected out under overdose anesthesia. Peripheral blood samples were also collected from the animals 3 months after transplantation to determine the chimeric ratio of blood cells.

Systemic Application of M-CSF

C57BL/6 (10 weeks of age, n = 5) mice received an intraperitoneal injection of M-CSF (Kyowa Hakko Kogyo, Tokyo, Japan) dissolved in physiological saline once per day for 7 consecutive days (total dose 7×10^5 units). The dose of M-CSF was equivalent to that used in a clinical setting, relative to body weight. On the day after M-CSF application, the temporal bones were collected and prepared for cryostat sections. Animals (n = 5) receiving physiological saline instead of M-CSF were used as controls.

Local Surgical Treatment

C57BL/6 mice (10 weeks of age) were injected with 3 μl physiological saline into the posterior semicircular canal (PSCC). This minimally invasive treatment was a modified protocol used in previous studies when administrating drugs (Lee et al., 2003; Nakagawa et al., 2003; Kim et al., 2005) or cells (Iguchi et al., 2003; Okano et al., 2006) into the inner ear of mice. With animals under general anesthesia with ketamine (75 mg/kg) and xylazine (9 mg/kg), a retroauricular incision was made in the left ear, and the PSCC was exposed. A small hole (approximately 180 μm in diameter) was made in the bony wall of the PSCC with a 26-G needle. A fused silica glass needle (170 μm outer diameter; EiCOM, Kyoto, Japan) was then inserted into the perilymphatic space of the PSCC, and the solution was injected at a rate of 1 μl/min for 3 min using a Micro Syringe Pump (EiCOM). The hole in the PSCC was plugged with connective tissue and covered with fibrin glue. On days 1 (n = 4), 7 (n = 5), and 28 (n = 5), the left temporal bones were collected and prepared as cryostat sections to study the density of Iba1-positive cells in the cochlea. Temporal bones collected from age-matched normal animals were used as preoperative controls (n = 5).

The auditory function of experimental animals was monitored by auditory brainstem response (ABR) recording as described previously (Shiga et al., 2005). ABRs were recorded before treatment and on days 1, 7, and 28 after surgery. Thresholds were determined for frequencies of 10, 20, and 40 kHz.

The mobilization of Iba1-positive cells from BM to the cochlea were also examined in BM chimeric mice (n = 8) that had received EGFP-labeled HSCs 3 months before. Four animals received a saline injection into the PSCC as described

above, and the cochleae were collected 7 days after surgery. The remaining four animals were preserved as controls, receiving no surgical treatment.

Immunohistochemistry

Under general anesthesia with ketamine and xylazine, animals were perfused intracardially with ice-cooled phosphate-buffered saline (PBS), followed by 4% paraformaldehyde in phosphate buffer. The temporal bones were collected and immersed in the same fixative for 4 hr at 4°C. The samples were decalcified with 10% EDTA in PBS and cryoprotected with 30% sucrose. Specimens were prepared as cryostat sections (10 μm in thickness). Midmodiolar sections were provided for histological analyses.

Cryostat sections were immersed in blocking solution containing 10% goat serum for 30 min and incubated with a primary antibody at 4°C overnight. Characteristics of BM-derived cells were examined by immunostaining for leukocyte common antigen CD45; ionized calcium binding adapter molecule 1 (Iba1), which is specific for microglia/macrophages (Imai et al., 1996); microglia/macrophage-specific glycoprotein F4/80; and macrosialin CD68, which is specifically expressed by tissue macrophages. Immunohistochemistry for Ki67, a nuclear protein expressed in proliferating cells, was performed on the BM chimeric mice to determine the proliferation of BM-derived cells in situ. The primary antibodies used in this study were rat anti-mouse CD45 (1:50; 30-F11; BD Pharmingen), rabbit anti-Iba1 (1:1,000; Wako Pure Chemicals, Osaka, Japan), rat anti-mouse F4/80 (1:10; Cl:A3-1; Serotec, Oxford, United Kingdom), rat anti-mouse CD68 (1:1,000; FA-11; Serotec), and rabbit anti-Ki67 (1:200; SP6; Lab Vision, Fremont, CA). The localization of primary antibodies was visualized using secondary antibodies conjugated with Alexa Fluor 488, 555, or 633 (1:500; Molecular Probes, Eugene, OR). Nuclei were counterstained by 4′,6-diamidino,2-phenylindole dihydrochloride (DAPI; 1 μg/ml in PBS; Molecular Probes). Negative controls lacked primary antibody labeling. Specimens were viewed with a Nikon Eclipse E600 fluorescence microscope (Nikon, Tokyo, Japan) or a Leica TCS-SP2 confocal laser scanning microscope (Leica Microsystems, Tokyo, Japan) with a digital image-capture system.

Quantification

To determine the chimeric ratio in peripheral blood, smears of blood samples were made on slides. Total cells with nuclei were based on nuclear counts with DAPI staining observed with a fluorescence microscope. The ratio of EGFP-positive cells to the total number of cells was calculated. At least 200 nuclei were counted in each sample.

For the quantitatification of BM-derived cells or Iba1-positive cells, four sections were selected randomly from the 12 most midmodiolar sections for each experimental or control animal. To assess the distribution of BM-derived cells in the cochlea, the number of cells derived from engrafted HSCs in one midmodiolar section from base to apex was counted in six animals at 6 months after HSC transplantation. All BM-derived cells defined by coexpression of EGFP and DAPI within the cochlea were counted by two double-blinded examiners. The number of HSC-derived cells coexpressing Iba1, F4/80, CD45, or CD68 was also counted for examination of the phenotype of BM-derived cells. The ratio of EGFP-positive cells labeled with Iba1, F4/80, CD45, or CD68 to the total number of EGFP-positive cells was calculated. To study the replacement of Iba1-positive cells in the cochlea by engrafted EGFP-positive cells, the number of cells dual-labeled with EGFP and Iba1 in one midmodiolar section was counted. The ratio of the expression of EGFP to the total number of Iba1-positive cells was calculated in the cochleae harvested at 1, 2, or 4 weeks and 3, or 6 months after HSC transplantation. To investigate the dynamics of EGFP- or Iba1-positive cells in the cochlea, the density of EGFP- or Iba1-positive cells in SG was calculated by a modified method as described previously for evaluating the density of SG neurons (Shinohara et al., 2002). All EGFP- or Iba1-positive cells with nuclei stained for DAPI within each profile of Rosenthal's canal from the midbasal portion of the cochlea were counted. The outline of Rosenthal's canal profile was then traced under a brightfield image to generate the area of SG in Image J software (http://www.nist.gov/lispix/imlab/prelim/dnld.html). The density of EGFP- or Iba1-positive cells in SG was expressed as the cell number for an area of 10,000 μm^2. The density of EGFP- or Iba1-positive cells in SL of midbasal portion of the cochlea was also calculated by tracing the outline of the SL region occupied by type I-V fibrocytes and expressed as the cell number for an area of 10,000 μm^2. The number of total cells in the area of interest was determined by counting nuclei on DAPI-stained sections in Image J software. The number of proliferating macrophages in the cochlea was determined by counting the colocalization of Ki67 and DAPI. The ratio of EGFP-positive cells labeled with Ki67 to the total number of CD68-positive cells per section was also calculated.

Statistcal Analysis

Statistical analyses were performed by using one-way analysis of variance (ANOVA) followed by the Tukey-Kramer's test, for the analysis of ABR thresholds, alteration of Iba1-positive cells by EGFP-positive cells, and effect of local surgical stress. An unpaired *t*-test was used in other statistical analyses. $P < 0.05$ was considered statistically significant. All data are presented as the mean ± SE.

RESULTS

BM-Derived Cells Are Widely Distributed in the Spiral Ganglion and the Spiral Ligament

Six months after BM transplantation, numerous EGFP-positive cells were found widely within the cochlea of transplanted mice (Fig. 1a). A large population of EGFP-positive cells is located in the connective tissue of SL and auditory nervous system, including SG and acoustic nerve (AN; Fig. 1b–d). In SL, EGFP-positive cells were observed predominantly in its lower portion, corresponding to the type II and IV fibrocyte regions (Fig. 1b). In the auditory nervous system, EGFP-positive cells were observed along nerve fibers both in SG and

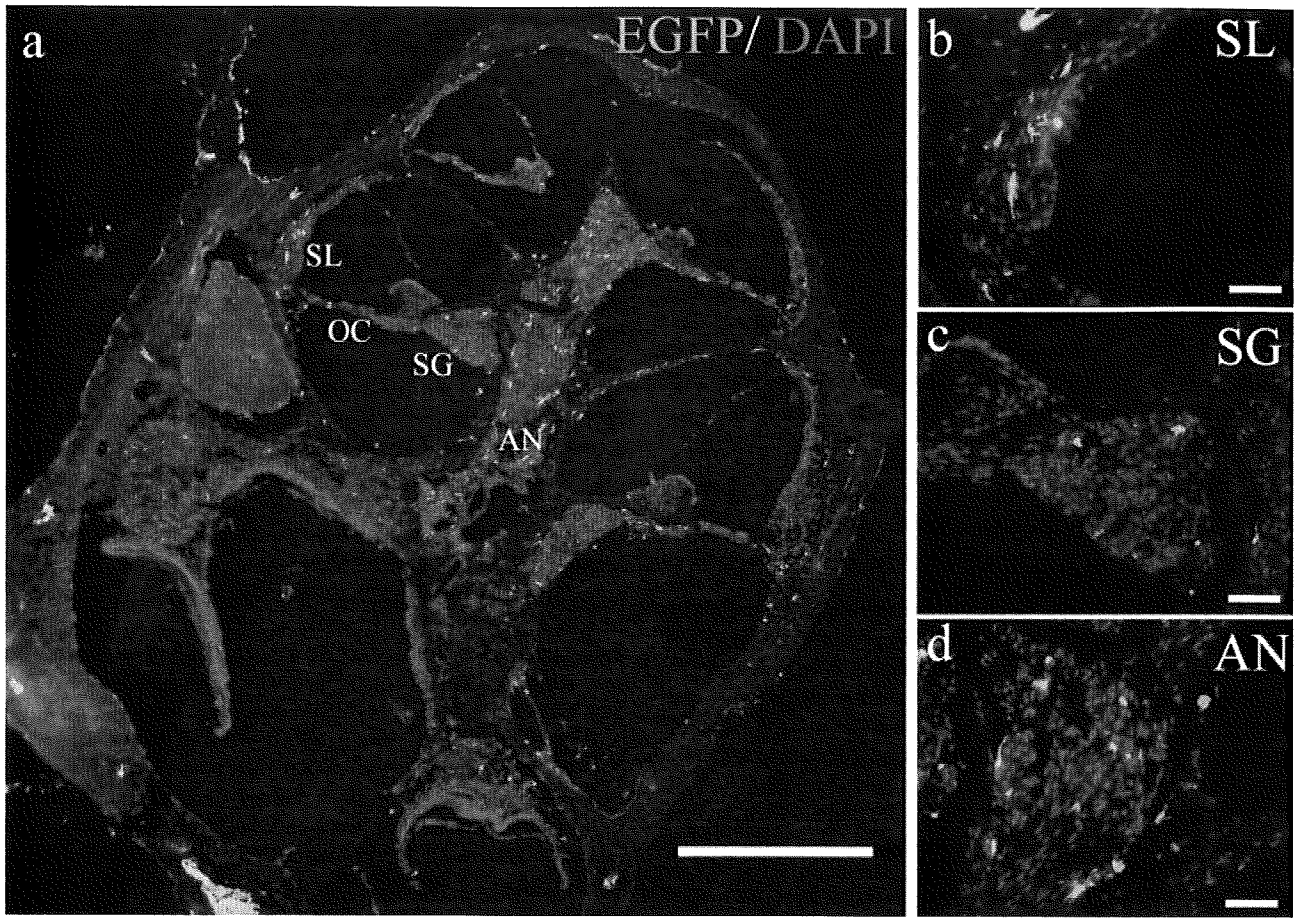

Fig. 1. Distribution of hematopoietic cell-derived cells in the cochlea. **a:** Distribution of hematopoietic cell-derived cells is shown in a midmodiolar section obtained from bone marrow (BM) chimeric mice 6 months after transplantation. BM-derived cells expressing EGFP were distributed from the base to the apex of the cochlea. Blue fluorescence shows nuclear staining with DAPI. **b–d:** In SL, EGFP-positive cells were observed predominantly in the lower portion of SL occupied by type II and IV fibrocytes (b). In the auditory nervous system, EGFP-positive cells were observed along nerve fibers in both SG (c) and cochlear modiolus (d). AN, auditory nerve; OC, organ of Corti; SG, spiral ganglion; SL, spiral ligament. Scale bars = 500 μm in a; 50 μm in b–d.

AN (Fig. 1c,d). In one midmodiolar section obtained at 6 months after transplantation, 90.3 ± 6.9 cells expressing EGFP were observed, 35.6% ± 3.1% of which were in the cochlear connective tissues of SL and the spiral limbus and 62.2% ± 3.0% in the cochlear nervous system, including SG and AN. The proportion of BM-derived cells to the total cells was 7.7% ± 0.9% in SL and 5.5% ± 0.9% in SG, which was compatible with the study by Lang et al. (2006). EGFP-positive cells were occasionally identified on the undersurface of the basilar membrane in the scala tympani and in the stria vascularis (data not shown). No EGFP-positive cells were observed within the cochlear sensory epithelium.

More Than 80% of BM-Derived Cells in the Cochlea Demonstrated the Phenotype of Macrophages

The following analyses of immunohistochemistry were carried out to characterize hematopoietic BM-derived cells in the adult mouse cochlea. Most EGFP-positive cells expressed F4/80 (Fig. 2a), Iba1 (Fig. 2b), or CD68 (Fig. 2c), indicating that cochlear HSC-derived cells have differentiated into the macrophage lineage. Cells dually labeled with EGFP and Iba1, EGFP, or F4/80 or with EGFP and CD68 were localized both in the cochlear connective tissue and the cochlear nervous system. The expression of Iba1 was found in 92.5% ± 3.1% of EGFP-positive cells, and F4/80 expression was observed in 87.3% ± 4.2%. Although more than 80% of BM-derived cells in the cochlea demonstrated the phenotype of macrophage, immunoreactivity for CD45, a common leukocyte antigen, was identified in only 7.4% ± 0.5% of EGFP-positive cells in the cochlea of BM chimeric mice. The number of cells doubly stained with Iba1 and CD45 was limited to one or two in one section (0.9% ± 0.3% of the total number of Iba1-positive BM-derived cells) except for cells in BM of the temporal bone. In contrast, CD68 expression was found in 81.7%

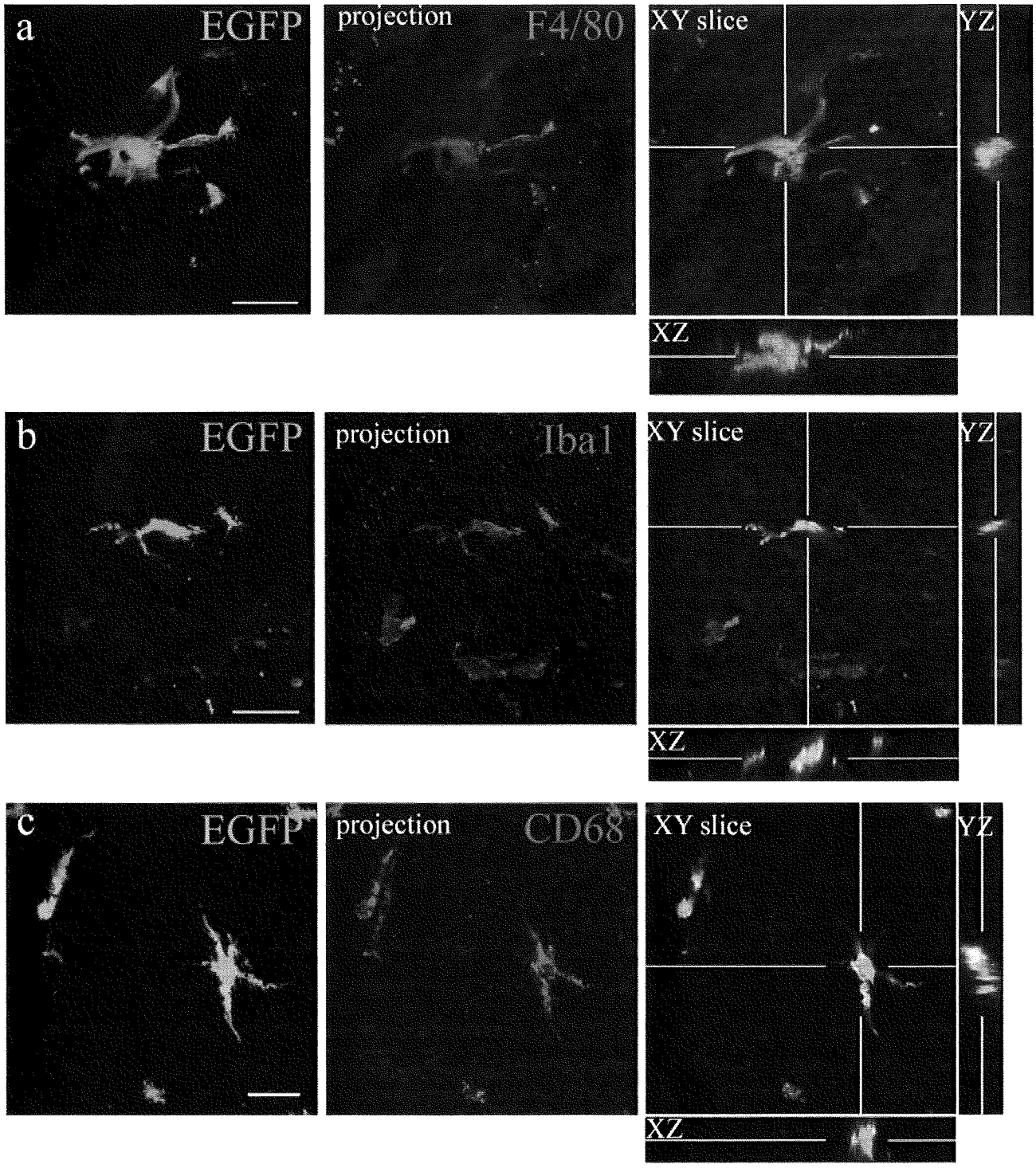

Fig. 2. Immunohistochemistry for F4/80, Iba1, and CD68 in the cochleae of bone marrow chimeric mice 6 months after transplantation. **a:** Photomicrographs obtained by confocal microscopy demonstrate colocalization of EGFP and F4/80 in the cells derived from transplanted HSCs within the spiral ganglion (SG). Immunoreactivity for F4/80 was frequently observed in HSC-derived cells in the lower part of spiral ligament (SL) and the SG. **b:** Iba1 expression was also found in HSC-derived cells in the SL and SG. With confocal microscopy, HSC-derived cells in SL are found to be dually labeled with EGFP and Iba1. **c:** CD68 was also colocalized in BM-derived cells expressing Iba1 in SL. Scale bars = 20 μm.